Mean Field Theory of Self-Organizing Memristive Connectomes

annalen der physik
www.ann-phys.org

Mean Field Theory of Self-Organizing Memristive Connectomes

Francesco Caravelli, Gianluca Milano, Carlo Ricciardi, and Zdenka Kuncic*

Biological neuronal networks are characterized by nonlinear interactions and complex connectivity. Given the growing impetus to build neuromorphic computers, understanding physical devices that exhibit structures and functionalities similar to biological neural networks is an important step toward this goal. Self-organizing circuits of nanodevices are at the forefront of the research in neuromorphic computing, as their behavior mimics synaptic plasticity features of biological neuronal circuits. However, an effective theory to describe their behavior is lacking. This study provides for the first time an effective mean field theory for the emergent voltage-induced polymorphism of circuits of a nanowire connectome, showing that the behavior of these circuits can be explained by a low-dimensional dynamical equation. The equation can be derived from the microscopic dynamics of a single memristive junction in analytical form. The effective model is tested on experiments of nanowire networks and show that it fits both the potentiation and depression of these synapse-mimicking circuits. It is shown that this theory applies beyond the case of nanowire networks by formulating a general mean-field theory of conductance transitions in self-organizing memristive connectomes.

1. Introduction

Unconventional physical systems consisting of many interacting components have been proposed for the realization of self-organizing and biologically plausible behavior where the response to electrical stimuli mimics features typical of neuronal circuits.[1]

Metallic nanowire (NW) networks are self-assembled networks of interconnected NWs that can be used for various applications, for instance in electronics,[2] energy storage,[3] sensors,[4] and machine learning.[5] Among metallic networks,[6,7] silver (Ag) NW networks have attracted great attention for the realization of neuromorphic devices and architectures,[1,5,8,9] as the electric field required to drive the dissolution/nucleation processes is lower than that required of other metals.[10,11] For this reason, silver is considered (with Cu) an electrochemically active material perfect for memristive devices, as it is prone to form *Ag+* ions which start to migrate across the memristive cell. The memristive behavior in memristive cells with an electrochemically active metal electrode is connected to the electrochemical metallization mechanism (ECM) of switching.[12]

Self-assemblies of NWs are intriguing complex physical systems,[13] formed by randomly dispersing NWs with diameter in the order of tens of nanometers on a substrate. A self-assembled Ag-NW network is shown in **Figure 1**a. It is evident that these form intricate patterns of connectivity. Despite the apparent complexity of these networks, models for the generation of these networks mimicking the realistic formation of the NW network have been proposed in the literature,[13–15] reproducing the almost 2D structure of the circuit, and local properties such as the graph-theoretic average degree, physically related to the average number of junctions associated to a nanowire. Additionally, the intersection between two NWs (as shown in Figure 1b) act as electrical junctions with all the nonlinear characteristics of a memristive component,[16–21] making these systems promising platforms for the realization of neuromorphic electronic systems.[22]

A memristive component is a one-port (two-terminal) device where the internal resistance state depends on the history of the applied voltage or current.[23] Two-terminal memristive devices are considered fundamental building blocks for the physical realization of artificial neural networks.[24] Memristors act as artificial synapses, and over the last few years, both ordered and

F. Caravelli
Theoretical Division (T-4)
Los Alamos National Laboratory
Los Alamos, NM 87545, USA
E-mail: caravelli@lanl.gov

G. Milano
Advanced Materials Metrology and Life Sciences Division
INRiM (Istituto Nazionale di Ricerca Metrologica)
Strada delle Cacce 91, Torino 10135, Italy

C. Ricciardi
Department of Applied Science and Technology
Politecnico di Torino
C.so Duca degli Abruzzi 24, Torino 10129, Italy

Z. Kuncic
School of Physics
University of Sydney
Sydney, New South Wales 2006, Australia

The ORCID identification number(s) for the author(s) of this article can be found under https://doi.org/10.1002/andp.202300090

DOI: 10.1002/andp.202300090

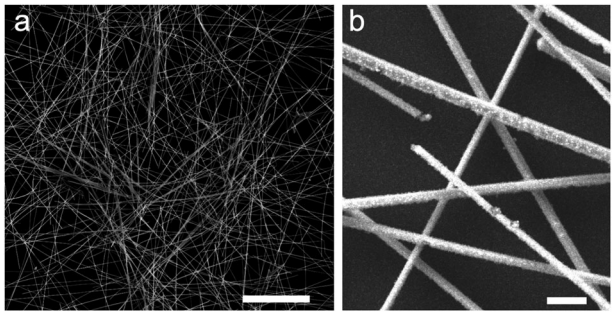

Figure 1. Connectome of a representative self-organizing nanowire network. a) SEM image of a network of highly interconnected Ag nanowires (scale bar, 10 μm); b) magnified area showing nanoscale cross-point junctions between intersecting NWs (scale bar, 400 nm).

disordered circuits of memristors have been studied theoretically and experimentally in the literature. Ordered networks of memristive devices, arranged in arrays of conventional crossbar architecture, have been used in a variety of supervised and unsupervised machine learning tasks, showing that these are apt for the implementation of brain-inspired computational frameworks.[25] However, it has been suggested in the literature that brain-inspired computation can also be achieved in disordered networks of memristive devices.[26] In particular, memristive devices can also be implemented using lithographically printed magnetic nanoislands, both in ordered and disordered arrays,[27,28] and tailored for computational purposes.[29,30]

In particular, memristive elements in these networks can endow short-term synaptic plasticity that is related to internal dynamics of memristive components,[31–34] making memristive NW networks suitable platforms for in material implementation of reservoir computing.[18,35] The wiring diagram of a large number of memristive nanowires forms an artificial *connectome*, for example, a network of nanowires and junctions. However, it is still unclear how collective dynamics and synaptic functionalities emerge coherently from such a complex connectome. As we show in this study, this is a property of memristive components arranged on a complex network.

The graph statistical properties of a connectome (such as the local number of connections) of NW network models have been studied in refs. [15, 36] together with emerging memristive dynamics,[13] providing a quantitative agreement with the existing experimental results within the context of Ag NW networks. The resistivity of these networks is mainly due to the voltage drop at the junctions (since $G_{\text{jun}} \ll G_{\text{wire}}$,[18]). This means that as a first approximation, one can neglect the resistivity of the wires and consider a network of ideal memristive junctions, whose behavior has to be then carefully analyzed. In the equivalent circuit, such approximation implies that Ag nanowires become effective nodes of the circuit, while junctions become memristive links. The key aspect of the present study is that the transition between low and high network conductance states can be described by a mean-field theory.

The interesting properties of Ag NW networks have been probed experimentally over the last decade.[8,9] The conductivity of the single junction and networks has been studied in detail, and its behavior emerges from the interplay of roughly two effects, depending on the composition of the wires. First, there are many geometrical effects, due to the distribution of the wires, which are not the scope of the present study. For instance, at low density of nanowires, there are few or no percolating paths between two nodes where the probes are attached. We are interested in the dynamic effects of conductivity, in particular, transitions between low and high conductance states.[8,14] In ref. [37], conductance transitions were predicted for circuits composed of the simplest type of memristive devices using the Strukov–Williams model for TiO_2 memristors,[23,38] which is a bulk model for filament conductance. The dynamical component is due to metal filament formation across the junction, due to the voltage-induced migration of Ag^+. Moreover, quantum tunneling also introduces a source of nonlinearity, but this becomes important only for nearly ungapped filaments.[14]

The internal dynamics of NW junction memristive elements characterized by short-term memory can be described by a rate-balance equation.[39] This is a dynamical model that can be used to describe the conductivity of the NW junction exhibiting a nonlinear dynamical response to a voltage bias, due to the formation of a metallic filament. For the type of Ag NW network experiments that we are interested in, the effective model which well describes the conductance of a single junction is a rate equation.[15,39] This dynamical model for the junction conductivity depends on two parameters, $G_{\min}$ and $G_{\max}$, representing the minimum and maximum conductance, and voltage-drop dependent rate constant η_P and η_D:

$$G(g) = G_{\min} g + G_{\max}(1-g) = G_{\min}(1+\chi g) \tag{1}$$

$$\frac{\mathrm{d}g}{\mathrm{d}t} = \eta_P(\Delta v)(1-g) - \eta_D(\Delta v) g \tag{2}$$

$$\eta_P(\Delta v) = \kappa_{P0} \exp(\eta_{P0} \Delta v) \tag{3}$$

$$\eta_D(\Delta v) = \kappa_{D0} \exp(-\eta_{D0} \Delta v) \tag{4}$$

Above, $G(g)$ is the junction conductance, g is the normalized conductance with $0 \le g \le 1$, Δv is the voltage drop on the junction. We have also introduced $\chi = (G_{\max} - G_{\min})/G_{\min}$, which can be interpreted as the degree to which the system presents memory effects. In fact, if $\chi = 0$, then these memristive elements become simple resistors. The parameter χ not only introduces then the nonlinearity in the system, but also induces the extent to which the system remembers the past states. Of course, in a circuit, the behavior of the conductance of the single junction is contained in the voltage drop Δv, and thus through the graph representing the circuit. In what follows, since we will have N junctions, we will refer to $\boldsymbol{G}(\vec{g})$ as the diagonal matrix of the conductances, and g_i the normalized conductance of the ith junction. The voltage drops Δv are generalized to a vector accordingly.

Disordered circuits such as those emerging in self-assembling nanowires present a variety of phenomena, and their architecture is closer to biological neuronal networks.[14,15] However, the fact that experimentally a rather similar behavior is observed in many differently self-assembled nano-structures suggests the existence of an underlying mechanism, such as self-averaging, explaining such homogeneity in responses. Overall, the underlying

complexity stands in the combination of spatiotemporal disorder, the nonlinear memory property of the single junction (cf. (2)), and the induced correlations between the junctions. In such a circuit, one has also to solve Kirchhoff laws. Let us call $\mathcal{G}$ the *directed* graph representing the circuit, with edges oriented according to the positive currents $\vec{i}$ in the junctions. The directionality is indeed artificial but can be chosen arbitrarily, so if the direction of the edge was chosen to be say +, then a negative current means a current going in the opposite orientation as chosen. We call B the directed incidence matrix of $\mathcal{G}$. Then, if the circuit is controlled by injecting a current between two nodes n_1, n_2, for example, $+|j|$ at n_1 and $-|j|$ at n_2, the Kirchhoff laws can be obtained by solving the nodal analysis equations

$$B\vec{i} = \vec{j}_{\text{ext}} \tag{5}$$

$$\boldsymbol{G}\Delta\vec{v} = \vec{i} \tag{6}$$

where $(j_{\text{ext}})_i = 0$ if $i \neq n_1, n_2$ and $(j_{\text{ext}})_i = \pm j$ for $i = n_1, n_2$ respectively. The matrix $\boldsymbol{G}$ represents the diagonal matrix with the corresponding conductance value, and thus Equation (6) simply represents Ohm's law in matricial form. We see then that in order to simulate a circuit of N junctions, we need to solve N dynamical equations from Equation (2) and $2N$ linear equations from Equation (6), and finally, calculate the effective conductance.

2. Results

Studying dynamical systems composed of many memristive systems is a cumbersome numerical process. The $3N$ equations of Equations (5) and (6) with Equations (1)–(4) require long numerical simulations, and do not provide a lot of room for simple interpretability of the results. It is however much simpler if we can obtain some results for the effective conductivity G_{eff} between the nodes n_1 and n_2 at which the probes are attached. This is the case in a typical experimental setup, in which the typical conductance measurement involves placing two probes between two (or more) nanowires. Thus, the quantity of interest is an effective resistance, which depends on the points of contact. Here, we use both analytical results and approximation methods to derive an effective mean field theory for the effective conductance. In the Methods section, we introduce the key results that lead to the derivation of the mean-field theory. For the purpose of context, we used the same analytical techniques introduced in refs. [37, 40, 41]. We first obtain an exact closed formula for the effective voltage drop at each junction (Lemma 1 and Corollary 1) by solving Kirchhoff's laws explicitly, reducing the system of equations from $3N$ to N. Then, we obtain an exact formula for the conductance (Corollary 2); however, it depends on the state of each single junction. We reduce the resulting N equations to a single one, using a mean field approximation (see Methods). Effectively, we show that the whole network can be reduced to an effective single junction model, similar in spirit to Equations (1)–(4). As a result, we obtain an effective internal junction conductance parameter $\langle g\rangle$, and the dynamical equations for the effective conductance can be written in terms of this quantity. As a result, our method allows us to describe the effective conductance measurement of this complex network of nanowires. The effective dynamical equations for the conductance are given by

$$G(\langle g\rangle) = G^{\text{eff}}_{\text{min}}(1 + \chi^{\text{eff}}\langle g\rangle) \tag{7}$$

$$\frac{\mathrm{d}\langle g\rangle}{\mathrm{d}t} = \eta^{\text{eff}}_{P}(\Delta v, \langle g\rangle)(1 - \langle g\rangle) - \eta^{\text{eff}}_{D}(\Delta v, \langle g\rangle)\langle g\rangle \tag{8}$$

$$\eta_P(\Delta v, \langle g\rangle) = \kappa^{\text{eff}}_{P0}\exp\left(\eta^{\text{eff}}_{P0}\frac{\Delta v}{1 + \chi^{\text{eff}}\langle g\rangle}\right) \tag{9}$$

$$\eta_D(\Delta v, \langle g\rangle) = \kappa^{\text{eff}}_{D0}\exp\left(-\eta^{\text{eff}}_{D0}\frac{\Delta v}{1 + \chi^{\text{eff}}\langle g\rangle}\right) \tag{10}$$

Above, $\langle g\rangle$ is an effective dynamical conductance parameter, which can be obtained from the microscopic values g_i of the single junctions via the mean field approximation. The specific expression for $\langle g\rangle$ in terms of the g_i and the circuit topology is not important from an effective macroscopic system perspective, as it is nonetheless self-consistent with the measurement of an initial value of the effective conductance of the sample.

It is important to note that the free parameters are of the same number as the ones for the single junction. The key difference is that now Δv is renormalized by a factor given by $1 + \chi^{\text{eff}}\langle g\rangle$; the other parameters are also renormalized by network-dependent quantities. Clearly, the equation above has the advantage that one uses a single rate equation for the entire NW network.

Our experimental results are based on measurements of a NW network device using two electrical probes.[15] Self-assembling NWs were realized by drop-casting Ag NWs in suspension on a SiO_2 insulating substrate.[43] A high density of NW cross-point junctions (106 junctions per mm^2) was achieved, ensuring that the network is above the percolation threshold. Ag NWs were passivated by a coating of PVP of 1–2 nm thickness around the Ag core.[15,18] PVP acts as a solid electrolyte for the junctions, as an electrochemical metallization induces a memristive behavior to the junction, characterized by the rate equation (Equation (2)). We then applied a square voltage of 2 V for 100 s, followed by a small voltage for measurement purposes, as shown in **Figure 2**a; using this protocol, we are measuring the short-term memory of the sample.

To see that the mean-field equation can fit the response of a real device, we consider the best-fit parameters that minimize, given the input voltage $\Delta v(t)$, the error $E_T = (\frac{1}{T}\int_0^T \mathrm{d}t(G^{\text{exp}}(t) - G^{mft}_{\text{eff}}(t)))^2$. As we can see from Figure 2a the mean-field theory reproduces the experimentally observed behavior of the network of junctions. Thus, it can be used to obtain, given the tuned parameters, the behavior of the nanowires as a function of the maximum voltage Δv applied to the device.

The advantage of using a mean-field equation such as Equation (8) is that, since it is 1D, we can always express it in terms of an effective potential V

$$\frac{\mathrm{d}\langle g\rangle}{\mathrm{d}t} = -\frac{\mathrm{d}V_{\Delta v}(\langle g\rangle)}{\mathrm{d}\langle g\rangle} \tag{11}$$

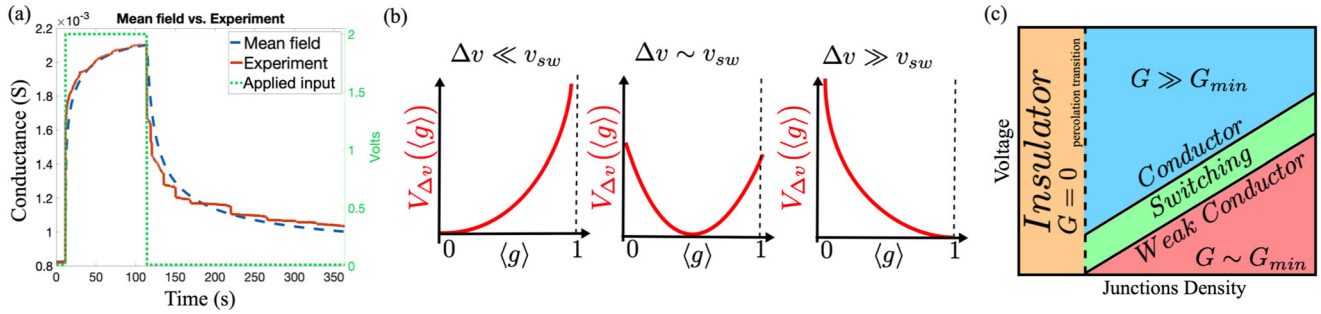

Figure 2. Effective mean-field behavior. a) Conductance response to a 2 V square signal, followed by a low readout voltage, delivered to an Ag-PVP NW network device (green, experimental data from ref. [5]) and mean-field theory fit of the experimental data (dashed blue).[42] b) Switching of the effective potential $V_{\Delta\nu}$ as a function of the order parameter $\langle g \rangle$ and applied voltage $\Delta\nu$. At low voltages, the system remains in a low conducting phase. At higher $\Delta\nu$, the potential switches, and the system becomes conductive. This behavior can be inferred from Equation (12). c) Schematic phase diagram of the system. At very low junction densities, the system does not have a conducting path. Above a percolation threshold, the system establishes a connected path and the conductance becomes a function of voltage. To the right of the insulating region, the system undergoes a phase transition as it switches to a conducting phase for a given density of memristive elements on the shortest path across the bias. This phase diagram depends on the initial conditions of the junctions; here we assume them to be all in the low-conductance state (i.e., homogeneous system). The diagram can indeed change for other systems and different initial conditions of the junctions, but we expect the general structure to be preserved.

that is, it shows that there is an effective low dimensional dynamics driven by a voltage-dependent mean-field potential $V_{\Delta\nu}$ (in the overdamped regime). This approach was previously applied to study current-controlled memristive circuits in ref. [37], where a change in symmetry of the potential occurs as a function of applied voltage. The theory was also recently extended to understand a larger class of dynamical systems involving projector operators.[56]

The effective potential can be obtained analytically by integrating Equation (8), giving $\mathrm{d}V_{\Delta\nu}(\langle g \rangle) = -\int \mathrm{d}\langle g \rangle \frac{\mathrm{d}\langle g \rangle}{\mathrm{d}t}$ (the exact expression is provided in Section SB2, Supporting Information). Let us, however, report here the phenomenology of the potential change. Using the effective parameters obtained from the fit in Figure 2a, we estimate that there is a threshold at which the potential switches and the system transitions from a low to a high conducting phase. The switching of the potential occurs at very small values of $\Delta\nu_{\mathrm{sw}}^{\mathrm{th}} \approx 2 \times 10^{-2}$ V. However, since the gradient is very shallow and it increases as a function of the voltage, a noticeable change in the effective conductance occurs, within the time scale of the tens-hundred seconds, for $\Delta\nu_{\mathrm{sw}}^{\mathrm{exp}} \approx 0.9$ V, which is consistent with the experimental timescale. The picture we obtain is then the one of Figure 2b, in which the potential changes its minimum abruptly, but continuously, for example, the equilibrium value of the effective conductance $\langle G_{\mathrm{eff}} \rangle^{\mathrm{eq}}$ changes from G_{min} to G_{max} as a function of $\Delta\nu$. As we can see, the effective description provides a qualitative and quantitative prediction of the conductance transition.

2.1. Conductance Transitions

As in the case of current controlled memristor networks studied in ref. [37], the effective potential can be calculated analytically via approximations. It ought to be noted, however, that there the potential switching takes a different form, and that unlike here, it is an unstable fixed point that moves as a function of the effective (average) current in the circuit. There, the system can have two stable fixed points at the same time. In our case instead, the system has always a single stable fixed point, which rapidly switches as a function of the applied voltages.

Nevertheless, the overall picture which emerges in both cases is similar and is the one shown in Figure 2c, replacing current with voltage. For sufficiently high circuit density (characterized by the number of memristive junctions), the mean-field description suggests that the system is in a low conductance state, and for larger applied voltages (or currents), the system switches to a high conductive state. This picture is qualitatively similar to other types of nanowire networks,[14] where it was found that threshold dynamics can lead to avalanches. These critical dynamics were also studied using mean-field theory in ref. [44].

It thus seems then that there is a general pattern emerging concerning nonlinear circuits with memory, for example, memristive circuits. At low densities of memristors, given the effective conductance between two nodes, the system is in an insulating phase because of the *geometric* features of the circuit. At higher densities, above a percolation threshold, the probability of establishing a conductance path between two nodes becomes macroscopically large, and would also occur in a resistor network. Our study is then concerned with the region to the right of this transition, where between a weak conducting and a conducting phase there is a switching region. Whilst the details of a such region depends on the type of memristor and initial conditions of the system, the results of this study (analytical) and[18] (numerical) for Ag nanowires, those of refs. [37, 40] for current controlled memristors (analytical), and those of ref. [14] for atomic switch NW networks[9] (numerical), suggest that such a phase diagram is robust to the details of the nonlinearity. this is because for low nodes the current flows on a smaller number of junctions, thus having a larger voltage drop on each, thus making them switch earlier.

It is important to stress that the mean-field theory presented in this study is a result of the symmetries induced by Kirchhoff's laws, and that can be applied to a variety of other systems. To see the broad applicability of this mean-field technique, we derived the equations for other models describing the dynamics of different self-organizing memristive networks. In fact, these

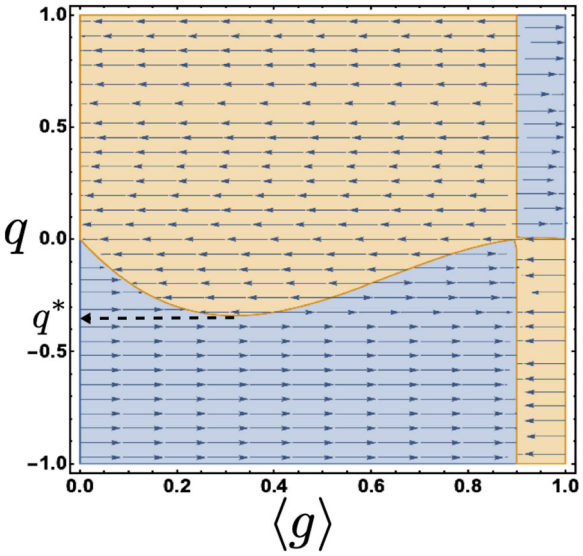

Figure 3. Effective force ($-\partial_z V(z)$) for the mean-field nano-particle/-wire filament formation in ref. [45], for $\kappa = a = 1$ as a function of the effective voltage q. For $q > 0$, the model is most likely in the low conductance state, but for values $q < q^*$ we observe an abrupt transition from a low to a high conductance state. The arrows show the directionality of the effective force, showing that it flips directions at a particular value of the driving voltage.

conductance transitions occur beyond a particular model; they were derived in ref. [37] for the case of TiO_2 memristor models, and to support the present study we derived mean-field equations for a model describing the behavior of both percolating nanoparticles[45] and 3D nanowires,[46] but still constrained by the Kirchhoff laws (see Methods).

We can thus immediately see why the conductance transitions are not a feature of a particular model. An analysis of the equations for the nanoparticles shows that there is a first-order transition between a high and low conductance state. This can be seen visually in **Figure 3**, where we plot the effective direction of the effective force driving the conductance parameter $\langle g \rangle$. As we can see, from the mean-field theory of this model we predict a first-order transition as a function of the effective voltage. This is the same phenomenon observed in refs. [14, 47] for a similar type of nanowire network. As we explain below, we contend this is a robust phenomenon that goes beyond the specific details of the model, and that can be characterized by an effective theory *a lá Landau*.

3. Effective Theory of Conductance Transitions

To understand when and how these conductance transitions occur, let us focus on the equilibrium obtained mean field equation for memristive nanowires, given by the solution of the equation (see Section SB1, Supporting Information)

$$\langle g \rangle^* = \left(1 + s e^{\frac{f_0 v}{1+\chi^{\text{eff}}}\langle g \rangle^*}\right)^{-1} \tag{12}$$

where the parameters f_0, s, and χ^{eff} can be determined experimentally, but have an explicit form from the mean-field theory in terms of the microscopic parameters. It can be seen explicitly from the equilibrium how the switching of Figure 2b occurs as a function of the applied voltage v.

For small values of v, the effective mean field potential takes the form

$$V(\langle g \rangle) = a\langle g \rangle + b\langle g \rangle^2 - cv \log(1 + \chi \langle g \rangle) \tag{13}$$

where a, b, and c are constants. In the case of the nanoparticles, such a potential can be written in the form

$$V(\langle g \rangle) = a\langle g \rangle^2 - bv \log(1 + f(\langle g \rangle)) \tag{14}$$

Similarly, for a network of memristors which satisfy $R(x) = R_{\text{on}} x + (1 - x) R_{\text{off}}$ and $\mathrm{d}x/\mathrm{d}t = -\alpha x + i/\beta$, the effective potential for the equivalent parameter $\langle x \rangle$ is given by[37]

$$V(\langle x \rangle) = \frac{\alpha}{2}\langle x \rangle^2 + \frac{v}{\chi} \log(1 - \chi \langle x \rangle) \tag{15}$$

In all these cases which can be studied analytically, we thus see that the general form of the potential is written in the form

$$V(\bar{r}) = \pm |Q(\bar{r}) - av \log\left(1 + P(\bar{r})\right)| \tag{16}$$

where $\bar{r}$ is a generic order parameter, and $Q(\cdot)$ and $P(\cdot)$ are generic functions, such that $Q(0) = Q'(0) = P(0) = 0$, that is, there are no constant terms and for $v = 0$ the only solution is $\bar{r} = 0$. The equilibrium points are then determined by the mean-field equation

$$\frac{\partial_{\bar{r}} Q(\bar{r})}{\partial_{\bar{r}} \log\left(1 + P(\bar{r})\right)} = av \tag{17}$$

If $P(\bar{r})$ is a monotonic function, we can always define the effective order parameter given by $s = \log(1 + P(\bar{r}))$ and then rewrite the expression above as the mean-field theory

$$Q(\bar{r}(s)) = \tilde{Q}(s) = avs \tag{18}$$

Using this formulation we see that the number of equilibrium points can be defined, as a function of the effective voltage v, *a lá Landau*, depending on the function $\tilde{Q}(s)$. For small values of v, there is only one fixed point $s = 0$, corresponding to the mean field parameter $\bar{r} = 0$. For larger values, depending on the function $\tilde{Q}(s)$, there can be multiple fixed points. However, if the function $\tilde{Q}(s)$ is globally convex, the transition is continuous, which is the situation described here, shown schematically in **Figure 4** (top). The order of the transition however depends on the shape of the function. First-order transitions can indeed occur if the function $\tilde{Q}(s)$ is non-convex, in which case one can have multiple equilibrium points, or even first-order transitions. These first-order transitions are indeed observed experimentally, for example, in ref. [14]. Using the mean field model, this situation is shown in Figure 4 (bottom).

One important issue is when and why the parameter χ is key to observing these transitions. Let us now extend here, to a more general case, the remarks made in ref. [37] about the role of χ. In that case, where we have $\chi = R_{\text{off}} - R_{\text{on}}/R_{\text{off}}$ (analogous to $\chi = (G_{\max} - G_{\min})/G_{\min}$ in this study), the parameter χ enters in the effective potential multiplying the function P. For instance, in the

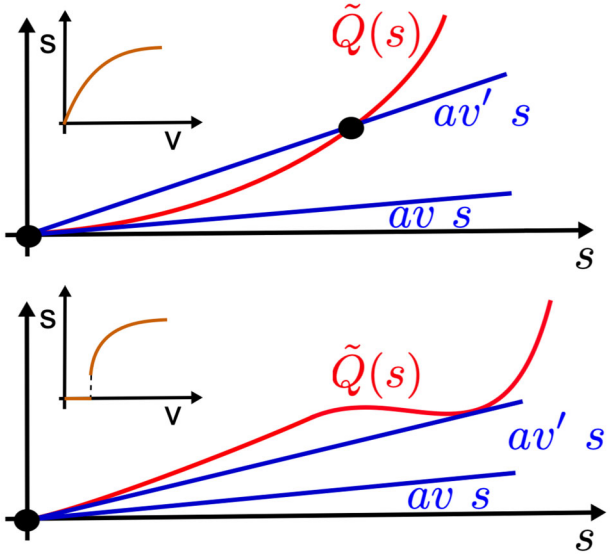

Figure 4. Graphical representation of Equation (18). (Top) For small values of the applied voltage v, because of the convexity of $Q(\bar{r})$ in 0, the only mean field parameter allowed equilibrium point is $\bar{r} = 0$, but as the voltage reaches a critical threshold, the system's effective order parameter s (e.g., equilibrium conductance) varies smoothly as a function of voltage (inset). (Bottom) For a non-convex function $\tilde{Q}(x)$, we can have first-order transitions as a function of the voltage (inset).

reported experiments of this study, we have $\chi \approx 100$. This implies that in the effective potential of Equation (18), it enters as

$$Q\left(P^{-1}\left(\frac{e^s - 1}{\chi}\right)\right) = avs \tag{19}$$

As a result, the larger the values of χ, the smaller the value of v at which these critical transitions occur. Since typically one has the constraint $\bar{r} \in [0, 1]$, one also must restrict the values of $s \in [s_{\max}, 0]$. This, in turn, restricts the values of χ, which explains why numerically one observes that there exists a minimum value χ^* in which these transitions occur. In this sense, the amount of memory in the system is an important quantity for these transitions to occur.

4. Discussion

The interplay between nonlinearity, Kirchhoff's laws, and memristive dynamics underlies the observed complex behavior of self-organizing memristive networks. Yet, as we show in this study, because of Kirchhoff's conservation laws much of this complexity can be, at least in the case of two-probe conductance measurements, reabsorbed into the effective parameters of a single junction. This drastic simplification is essentially due to the properties of projector operators.

In the present study, we derived an effective mean-field equation describing the behavior of the effective conductance of a NW network, and the effective equations for a network of nanoparticles. As we have seen, the dynamical behavior of the effective conductance of a NW network can be well approximated by a mean-field theory, derived from the microscopic equations describing memristive dynamics of a single junction, and the Kirchhoff laws. This is a model that succinctly characterizes the global switching behavior of a memristive NW network. For the case of the experiments presented in this study, it is important to note that the mean-field reduces the system of equations from $4N$ for the case of N junction, to simply four, and only four numbers of free parameters. As a result, this study shows that the application of these graph theoretical techniques to a complex system of self-organized NWs provides a quantitative explanation of the response of the system to an applied voltage.

However, most importantly it shows that conductance transitions in NW networks can be explained via the use of effective mean field potentials inspired by the Landau theory of phase transitions. This result is the latest addition to a series of papers[14,37] showing that there exists a typical phase diagram for the asymptotic conductance or resistance versus applied voltage or current. Whilst the details of the switching region depend on the system under scrutiny, we contend that the seemingly universal properties of these phase diagrams warrant further investigation. As we have shown analytically and with minimal assumptions, the behavior of the system to the applied voltage can be cast in the form of a standardized mean field equation. The continuous or discontinuous behavior of the conductance of the nanowire connectome is in fact connected to the convexity of the effective potential as a function of the voltage. In particular, we have also provided an analytical explanation for the reason why it is a *generic* feature that these transitions occur in systems with large memory, that is, when the range of the effective conductance of the system is large. As a result, this study opens a new way of analyzing and classifying the behavior of a generic memristive connectome in terms of the standard theory of phase transitions.

It is worth also mentioning that our graph theoretical techniques have a range of applicability beyond nanowire and nanoparticle networks. For instance, slime molds such as physarum polycephalum,[48–50] which inspired a variety of optimization algorithms,[51,52] can indeed be formulated as a memristive component with constraints given by network Kirchhoff's laws induced by the mapping between an incompressible fluid flow and electrical circuits.

While this work attempts to provide a mean-field theory treatment to memristive devices, it is worth mentioning that the mean-field theory in ref. [37] showed the existence of symmetry breaking, while it seems to be absent in our treatment of memristive nanowires. It is also worth mentioning that our method works within the approximation of discrete memristive junctions, with a voltage drop that can be quantified by a low-dimensional model for the conductance evolution (in our case, one parameter g). In this framework, it is important to point out that the dynamic behavior of memristive elements composing the network is described by means of a model that, while capturing the main features of dynamics, does not take into account quantum conductance effects that can result in discrete levels of conductance.[53] Additionally, the model does not take into account disorder due to variability effects in the initial pristine state and in the memristive response of network elements. Despite these assumptions, the mean-field theory approach is able to describe the main features of the emergent connectome behavior.

In general, while the models we considered in this study are valid for specific initial conditions of both the nanowire and the

nanoparticle states, and within the approximation of homogeneous properties of the single junctions, as discussed there is a general message that can be evinced from the study of physically relevant connectome models, also based on the discussion of the memristive network toy model introduced in ref. [37]. It is however thus important to stress that more work is needed to bring all these systems into a single theoretical framework. In principle, our techniques could be extended to more complex models such as the one proposed in ref. [54], with a continuous family of parameters. Both these extensions will be the scope of future investigations.

5. Methods

One of the key advancements of this study is a technical intermediate step that allows integrating analytically the Kirchhoff laws of Equations (5) and (6). In order to derive a mean-field equation, we use a graph theoretical formalism to formally evaluate Kirchhoff's laws. We call $\tilde{\mathcal{G}} = \mathcal{G} \cup \mathcal{G}_{n_1 n_2}$, for example, the graph with the single edge $\mathcal{G}_{n_1 n_2} = (n_1, n_2)$ added to the graph. Formally, it is possible to convert the current $\vec{j}_{\text{ext}}$ into an external voltage source v_{N+1}, in series to a conductance G_{N+1}, and satisfying $G_{N+1} v_{N+1} = j$. Since we now have $N+1$ voltage drops in the circuit, the vector of all voltage drops is given by Δv_{all}, where the first N components were $\Delta\vec{v}$ and the $(N+1)$th component is the voltage drop on the voltage source branch. As we show in the Supporting Information (Section SA, Supporting Information), we can write $\vec{j}_{\text{ext}} = G_{N+1}\tilde{B}\vec{v}_s$, where $(\vec{v}_s)_i = 0$ for $i \neq n_1, n_2$ and $(\vec{v}_s)_i = \pm v_{N+1}/2$ for $i = n_1, n_2$, respectively. The parameter g_{N+1} must satisfy $G(g_{N+1}) = G_{N+1}$, and it could be shown that $\lim_{G_{N+1}\to 0} g_{N+1} = -\frac{1}{\chi}$.

Let $\tilde{\mathcal{G}}$ be the augmented graph with an extra directed edge between node n_1 and n_2, and $\tilde{B}$ the corresponding directed incidence matrix. As shown below, the voltage drops can be found analytically, thus avoiding solving numerically for Equations (5) and (6). In fact, we have (see Section SA1, Supporting Information):

Lemma 1 (Network voltage integration). *For a circuit composed of memristive junctions satisfying Equation (1), we have the following identity*

$$\Delta\vec{v}_{all} = \lim_{G_{N+1}\to 0} \frac{G_{N+1}}{G_{min}} (I + \chi\Omega\mathbf{g})^{-1}\Omega\vec{v}_s \tag{20}$$

where $\Omega = \tilde{B}^t(\tilde{B}\tilde{B}^t)^{-1}\tilde{B}$ is a projector operator and $\mathbf{g}$ is the diagonal matrix $diag(\vec{g}, g_{N+1})$. The relevance of Equation (20) is that Kirchhoff's laws have been integrated analytically. The underlying physical reason for the introduction of a projector operator, which has the property $\Omega^2 = \Omega$, is that it enforces the conservation of currents at the nodes.[41] The matrix $\tilde{B}$ is the directed incidence matrix of the augmented graph $\tilde{\mathcal{G}}$ (see Figure S2, Supporting Information in Section SA, Supporting Information), in which we have added an extra edge where either the voltage or current generator has been added. The matrix Ω, which represents the interactions between elements due to Kirchhoff's laws, has been studied in detail previously.[40] In the case of planar circuits, for example, it was found that the interactions fall off exponentially with distance.[55]

It is important to mention that Equation (20) is useful since we can obtain both the voltage drops for the single junctions, which we can insert in Equation (2) to time evolve the conductances and to obtain the effective behavior of the memristive network. In fact, the $N+1$ component of Equation (20) must satisfy the equation $\Delta v_{N+1} G_{\text{eff}} = j$. Thus, one has to separate the matrix inverse of Equation (20) in blocks. In order to do that, first we divide Ω on the subgraphs $\mathcal{G}$ and $\mathcal{G}_{n_1 n_2}$ as

$$\Omega = \begin{pmatrix} \tilde{\Omega} & \vec{\Omega} \\ \vec{\Omega}^t & \Omega_{N+1} \end{pmatrix} \tag{21}$$

Let us define the quantity

$$\rho = \Omega_{N+1} - \chi\vec{\Omega}^t\tilde{\mathbf{g}}(I + \chi\tilde{\Omega}\tilde{\mathbf{g}})^{-1}\vec{\Omega} \tag{22}$$

where $\tilde{\mathbf{g}} = \text{diag}(\vec{g})$, for example, the parameters associated with the junctions. Let us now give a physical interpretation of these two quantities.

From the definitions above, we proved the following Corollaries (See Section SA, Supporting Information, Sections 4 and 6):

Corollary 1 (Voltage drops). *Let $\tilde{G}$ be an augmented circuit composed of memristive junctions of the form of Equation (1). Then the voltage drops on the junctions are given by*

$$\Delta\vec{v} = \frac{v_{N+1}}{1-\rho}\frac{G_{N+1}}{G_{min}}(I + \chi\tilde{\Omega}\tilde{\mathbf{g}})^{-1}\vec{\Omega} \tag{23}$$

We can also extract the effective conductance, and we have

Corollary 2 (Effective conductance). *Let $\tilde{G}$ be an augmented circuit composed of memristive junctions of the form of Equation (1). Then the effective conductance between node n_1 and n_2 is given by*

$$G_{eff} = G_{min}\frac{1 + \chi g_{N+1}\rho}{\rho} \tag{24}$$

We see that Corollary 1 and Corollary 2 are formal statements regarding the voltage drops and effective resistance as a function of the parameters $\vec{g}$ and the circuit topology, contained in Ω. The Lemma and Corollaries above can also be generalized to nonlinear conductance functions, and we will see an example below and in Supporting Information.

Let us provide a brief interpretation of Equation (23). The vector $\vec{\Omega}$ can be thought of as a network backbone of the response function, for example, the effective voltage on junction i must be proportional to $(\vec{\Omega})_i$. Effectively, Equation (23) is the solution of the voltage integration across the network, starting from the assumption that the voltage is applied between two nodes, inducing the separation of the matrix Ω given in Equation (21). The matrix $\tilde{\Omega}$ enters instead in the matrix inverse multiplying the internal junction conductances. Instead, Equation (24) is important as it provides an interpretation of the quantity ρ defined in Equation (22) in terms of global effective conductance.

However, these are static statements, which do not take into account the fact that the junction conductances change over time. To derive an effective mean-field theory, we introduce an effective mean-field variable $\langle g(t)\rangle$ for the junction conductances.

5.1. Mean-Field Approximation

All the equations above are exact. However, we can see that we are still left with a matrix inverse given by $(I + \chi\tilde{\Omega}\tilde{g})^{-1}$. In order to simplify the equations and obtain a lower-dimensional system, we define the mean-field variable $\langle g\rangle$ via

$$\langle g\rangle = \text{argmin}_{\tilde{g}} \|(I + \chi\tilde{\Omega}\tilde{g}) - (I + \tilde{g}\chi\tilde{\Omega})\|_F^2 \tag{25}$$

where $\|\|_F^2$ represents the Frobenius matrix norm-squared, that is, $\|M\|_F^2 = \text{Tr}(MM^t)$. It is indeed easy to see that if it minimizes the function above, it also minimizes a similar definition with the matrix inverses. The exact solution is given by $\langle g\rangle = \frac{\text{Tr}(\tilde{\Omega}^2 g)}{\text{Tr}(\tilde{\Omega}^2)}$. The result is thus a complex function defined in terms of the single junction parameters $\vec{g}$, and the network connectivity. This might seem at first a drawback, as the mean-field parameter we are interested in is defined in terms of a large number of unknown parameters, including the network topology. However, as we show below, if we assume that such a mean-field order parameter exists, we reduce the number of parameters to be fit experimentally to only four plus $\langle g\rangle$; these can then be fit experimentally. First, it can be shown that

$$G_{\text{eff}}(\langle g\rangle) = \frac{1 - \Omega_{N+1}}{\Omega_{N+1}} G(\langle g\rangle) \tag{26}$$

We thus have that depending on where the external voltage (or current) generator simply is reabsorbed into the G_{min} and G_{max} parameters, and the conductance parameters can be fit experimentally using the same model. The voltage for each memristive junction is given, in the mean-field approximation, by

$$\Delta\vec{v} \approx \Delta\vec{v}_{mft} = \frac{G_{N+1} v_{N+1}}{G_{\text{min}}(1 - \Omega_{N+1})} \frac{1}{1 + \langle g\rangle\chi}\vec{\Omega} \tag{27}$$

where the vector $\vec{\Omega}$ represents the response of each memristive element when a voltage is applied to the network between nodes n_1 and n_N. We now perform the second approximation. We replace $\vec{\Omega}$ with $\langle\Omega\rangle\vec{1}$. Then, at this point summing cleverly on the left-hand side gives a self-consistent *single* memristor equation (details in Section SC, Supporting Information), in which the parameters η_P, η_D, κ_P, and κ_D are multiplied by network-dependent quantities. The applied voltage is instead multiplied by a factor

$$\Delta v \to \Delta v/(1 + \chi^{\text{eff}}\langle g\rangle) \tag{28}$$

We thus see that by putting all these intermediate results together, we do obtain an effective system of equations as those in Equations (1) and (2).

5.2. Other Memristive Systems

For the case of the model introduced in ref. [46], we consider the following model for the conductance $G(z)$ of each junction, given by the set of equations

$$\frac{dz}{dt} = \mu\frac{V}{D - z} - \kappa z,\ G(z) = \alpha e^{-\beta(D-z)} \tag{29}$$

with $\mu = 0.346\ \text{nm}^2\ \text{V}^{-1}$ and $\kappa = 0.038\ \text{s}^{-1}$. D is the distance between the nanoparticles or nanowires (in nm) and $z(t)$ represents the effective gap between the evolving nano-filament and the nano-wire/-particle. In the Supporting Information (in Section SB, Supporting Information) we have obtained a generalization of Lemma 1 in Methods, and the subsequent corollaries to the case of a junction whose conductance is not a linear function of the internal memory parameter g.

We provide here the necessary background to understand the model of ref. [46]. Similarly to what we had done before, we rewrite the equations above in terms of a single parameter $g = z/D$. Then, the effective mean-field can be obtained by imposing $\vec{g} = \langle g\rangle\vec{1}$. and we obtain the effective equations (see Section SB, Supporting Information)

$$\frac{d}{dt}\langle g\rangle = \frac{q_{\text{eff}}}{\big(1 - \langle g\rangle\big)\big(1 + \chi_{\text{eff}} f(\langle g\rangle)\big)} - \kappa_{\text{eff}}\langle g\rangle \tag{30}$$

$$G_{\text{eff}}(\langle g\rangle) = G_{\text{min}}^{\text{eff}}\ (1 + \chi_{\text{eff}} f(\langle g\rangle)) \tag{31}$$

with $f(x) = e^{-a(1-x)} - 1$ and $\chi_{\text{eff}} = (G_{\text{max}}^{\text{eff}} - G_{\text{min}}^{\text{eff}})/G_{\text{min}}^{\text{eff}}$. Above, $q_{\text{eff}} = av$, where a is a proportionality constant depending on the microscopic parameters, while v is an effective voltage.

Supporting Information

Supporting Information is available from the Wiley Online Library or from the author.

Acknowledgements

The work of F.C. was conducted under the auspices of the National Nuclear Security Administration of the United States Department of Energy at Los Alamos National Laboratory (LANL) under Contract No. DE-AC52-06NA25396 (LANL Laboratory Directed Research Development 20200105ER)

Conflict of Interest

The authors declare no conflict of interest.

Author Contributions

F.C. derived the equations and wrote the initial draft. G.M. performed the experiments. All authors contributed equally to the study conception and design, and to the writing of the manuscript.

Data Availability Statement

The data and fit of Figure 3 are available on FigShare.[42] All other data are available within the manuscript.

Keywords

conductance transitions, mean field theory, memristors, silver nanowires

Received: March 12, 2023
Revised: May 7, 2023
Published online: June 6, 2023

[1] Z. Kuncic, T. Nakayama, *Adv. Phys.: X* **2021**, *6*, 1894234.
[2] C. Jia, Z. Lin, Y. Huang, X. Duan, *Chem. Rev.* **2019**, *119*, 9074.
[3] K. Yu, X. Pan, G. Zhang, X. Liao, X. Zhou, M. Yan, L. Xu, L. Mai, *Adv. Energy Mater.* **2018**, *8*, 1802369.
[4] F. Patolsky, C. M. Lieber, *Mater. Today* **2005**, *8*, 20.
[5] G. Milano, G. Pedretti, K. Montano, S. Ricci, S. Hashemkhani, L. Boarino, D. Ielmini, C. Ricciardi, *Nat. Mater.* **2022**, *21*, 195.
[6] E. Garnett, L. Mai, P. Yang, *Chem. Rev.* **2019**, *119*, 8955.
[7] S. I. Kim, J. H. Lee, Y. W. Chang, K.-H. Yoo, in *2010 3rd Int. Nanoelectronics Conf. (INEC)*, IEEE, Piscataway, NJ **2010**, pp. 1126–1127.
[8] A. Diaz-Alvarez, R. Higuchi, P. Sanz-Leon, I. Marcus, Y. Shingaya, A. Z. Stieg, J. K. Gimzewski, Z. Kuncic, T. Nakayama, *Sci. Rep.* **2019**, *9*, 14920.
[9] A. Avizienis, H. Sillin, C. Martin-Olmos, H. Shieh, M. Aono, A. Stieg, J. Gimzewski, *PLoS One* **2012**, *7*, e42772.
[10] Y. Yang, P. Gao, L. Li, X. Pan, S. Tappertzhofen, S. Choi, R. Waser, I. Valov, W. D. Lu, *Nat. Commun.* **2014**, *5*, 4232.
[11] Z. Kuncic, T. Nakayama, J. Gimzewski, *Neuromorphic Comput. Eng.* **2022**, *2*, 040201.
[12] I. Valov, R. Waser, J. R. Jameson, M. N. Kozicki, *Nanotechnology* **2011**, *22*, 254003.
[13] R. Zhu, J. Hochstetter, A. Loeffler, A. Diaz-Alvarez, T. Nakayama, J. T. Lizier, Z. Kuncic, *Sci. Rep.* **2021**, *11*, 13047.
[14] J. Hochstetter, R. Zhu, A. Loeffler, A. Diaz-Alvarez, T. Nakayama, Z. Kuncic, *Nat. Commun.* **2021**, *12*, 4008.
[15] G. Milano, E. Miranda, C. Ricciardi, *Neural Networks* **2022**, *150*, 137.
[16] G. Milano, S. Porro, I. Valov, C. Ricciardi, *Adv. Electron. Mater.* **2019**, *5*, 1800909.
[17] H. G. Manning, F. Niosi, C. G. da Rocha, A. T. Bellew, C. O'Callaghan, S. Biswas, P. F. Flowers, B. J. Wiley, J. D. Holmes, M. S. Ferreira, J. J. Boland, *Nat. Commun.* **2018**, *9*, 3219.
[18] G. Milano, G. Pedretti, M. Fretto, L. Boarino, F. Benfenati, D. Ielmini, I. Valov, C. Ricciardi, *Adv. Intell. Syst.* **2020**, *2*, 2000096.
[19] K. Nagashima, T. Yanagida, K. Oka, M. Kanai, A. Klamchuen, J.-S. Kim, B. H. Park, T. Kawai, *Nano Lett.* **2011**, *11*, 2114.
[20] L. He, Z.-M. Liao, H.-C. Wu, X.-X. Tian, D.-S. Xu, G. L. W. Cross, G. S. Duesberg, I. V. Shvets, D.-P. Yu, *Nano Lett.* **2011**, *11*, 4601.
[21] Y. Yang, X. Zhang, M. Gao, F. Zeng, W. Zhou, S. Xie, F. Pan, *Nanoscale* **2011**, *3*, 1917.
[22] C. Mead, *Proc. IEEE* **1990**, *78*, 1629.
[23] D. B. Strukov, G. S. Snider, D. R. Stewart, R. S. Williams, *Nature* **2008**, *453*, 80.
[24] Y. Zhang, Z. Wang, J. Zhu, Y. Yang, M. Rao, W. Song, Y. Zhuo, X. Zhang, M. Cui, L. Shen, R. Huang, J. J. Yang, *Appl. Phys. Rev.* **2020**, *7*, 011308.
[25] Q. Xia, J. J. Yang, *Nat. Mater.* **2019**, *18*, 309.
[26] F. Caravelli, J. Carbajal, *Technologies* **2018**, *6*, 118.
[27] M. Saccone, F. Caravelli, K. Hofhuis, S. Parchenko, Y. A. Birkhölzer, S. Dhuey, A. Kleibert, S. van Dijken, C. Nisoli, A. Farhan, *Nat. Phys.* **2022**, *18*, 517.
[28] F. Caravelli, G.-W. Chern, C. Nisoli, *New J. Phys.* **2022**, *24*, 023020.
[29] F. Caravelli, C. Nisoli, *New J. Phys.* **2020**, *22*, 103052.
[30] J. C. Gartside, K. D. Stenning, A. Vanstone, H. H. Holder, D. M. Arroo, T. Dion, F. Caravelli, H. Kurebayashi, W. R. Branford, *Nat. Nanotechnol.* **2022**, *17*, 460.
[31] R. S. Zucker, W. G. Regehr, *Annu. Rev. Physiol.* **2002**, *64*, 355.
[32] T. Ohno, T. Hasegawa, A. Nayak, T. Tsuruoka, J. K. Gimzewski, M. Aono, *Appl. Phys. Lett.* **2011**, *99*, 203108.
[33] Z. Wang, S. Joshi, S. E. Savel'ev, H. Jiang, R. Midya, P. Lin, M. Hu, N. Ge, J. P. Strachan, Z. Li, Q. Wu, M. Barnell, G.-L. Li, H. L. Xin, R. S. Williams, Q. Xia, J. J. Yang, *Nat. Mater.* **2016**, *16*, 101.
[34] G. Milano, M. Luebben, Z. Ma, R. Dunin-Borkowski, L. Boarino, C. F. Pirri, R. Waser, C. Ricciardi, I. Valov, *Nat. Commun.* **2018**, *9*, 5151.
[35] F. C. Sheldon, A. Kolchinsky, F. Caravelli, *Phys. Rev. E* **2022**, *106*, 045310.
[36] A. Loeffler, R. Zhu, J. Hochstetter, M. Li, K. Fu, A. Diaz-Alvarez, T. Nakayama, J. M. Shine, Z. Kuncic, *Front. Neurosci.* **2020**, *14*, 184.
[37] F. Caravelli, F. C. Sheldon, F. L. Traversa, *Sci. Adv.* **2021**, *7*, abh1542.
[38] J. J. Yang, D. B. Strukov, D. R. Stewart, *Nat. Nanotechnol.* **2012**, *8*, 13.
[39] E. Miranda, G. Milano, C. Ricciardi, *IEEE Trans. Nanotechnol.* **2020**, *19*, 297.
[40] F. Caravelli, F. L. Traversa, M. Di Ventra, *Phys. Rev. E* **2017**, *95*, 022140.
[41] A. Zegarac, F. Caravelli, *Europhys. Lett.* **2019**, *125*, 10001.
[42] F. Caravelli, G. Milano, C. Ricciardi, Z. Kuncic, figshare, **2023**, https://figshare.com/articles/software/Mean_field_theory_of_self-organizing_memristive_connectomes_-_Data_and_Fit/22746596 (accessed: April 2023).
[43] G. Milano, G. Pedretti, M. Fretto, L. Boarino, F. Benfenati, D. Ielmini, I. Valov, C. Ricciardi, *Adv. Intell. Syst.* **2020**, *2*, 2000096.
[44] F. C. Sheldon, M. Di Ventra, *Phys. Rev. E* **2017**, *95*, 012305.
[45] A. Sattar, S. Fostner, S. A. Brown, *Phys. Rev. Lett.* **2013**, *111*, 136808.
[46] R. K. Daniels, J. B. Mallinson, Z. E. Heywood, P. J. Bones, M. D. Arnold, S. A. Brown, *Neural Networks* **2022**, *154*, 122.
[47] M. D. Pike, S. K. Bose, J. B. Mallinson, S. K. Acharya, S. Shirai, E. Galli, S. J. Weddell, P. J. Bones, M. D. Arnold, S. A. Brown, *Nano Lett.* **2020**, *20*, 3935.
[48] T. Nakagaki, H. Yamada, A. Tóth, *Nature* **2000**, *407*, 470.
[49] A. Tero, T. Kobayashi, T. Nakagaki, *J. Theor. Biol.* **2007**, *244*, 553.
[50] K. Alim, N. Andrew, A. Pringle, M. P. Brenner, *Proc. Natl. Acad. Sci. U. S. A.* **2017**, *114*, 5136.
[51] A. Adamatzky, *Bioevaluation of World Transport Networks*, World Scientific, Singapore **2012**.
[52] V. Bonifaci, K. Mehlhorn, G. Varma, *J. Theor. Biol.* **2012**, *309*, 121.
[53] G. Milano, M. Aono, L. Boarino, U. Celano, T. Hasegawa, M. Kozicki, S. Majumdar, M. Menghini, E. Miranda, C. Ricciardi, S. Tappertzhofen, K. Terabe, I. Valov, *Adv. Mater.* **2022**, *34*, 2201248.
[54] W. Wang, M. Wang, E. Ambrosi, A. Bricalli, M. Laudato, Z. Sun, X. Chen, D. Ielmini, *Nat. Commun.* **2019**, *10*, 81.
[55] F. Caravelli, *Phys. Rev. E* **2017**, *96*, 052206.
[56] F. Caravelli, F. L. Traversa, M. Bonnin, F. Bonani, *Physica D: Nonlinear Phenomena* **2023**, *450*, 133747.